

# Learning to classify with possible sensor failures

Tianpei Xie, Nasser M. Nasrabadi, *Fellow, IEEE*, and Alfred O. Hero, *Fellow, IEEE*

**Abstract**—In this paper, we propose a general framework to learn a robust large-margin classifier, when corrupt measurements caused by sensor failure might be present in the training set. The goal is to minimize the generalization error of the classifier under the null hypothesis that the underlying distribution is nominal, with the constraint that the given hypothesis test has a false alarm rate less than a fixed threshold. By incorporating a non-parametric regularizer based on an empirical entropy estimator, we propose a Geometric-Entropy-Minimization regularized Maximum Entropy Discrimination (GEM-MED) method to perform classification and anomaly detection in a joint manner. We demonstrate that our proposed method can yield improved performance over previous robust classification methods in terms of both classification accuracy and anomaly detection rate using simulated data and real footstep data.

**Index Terms**—sensor failure, robust large-margin training, anomaly detection, maximum entropy discrimination.

## I. INTRODUCTION

Large margin classifiers, such as support vector machine (SVM) [1] and maximum entropy discrimination (MED) [2], have enjoyed great popularity among signal processing and machine learning communities due to their broad applicability, good performance, and the availability of fast implementation algorithms. When the training data is representative of the test data, the performance of SVM methods has theoretical guarantees that are validated in practice [1], [3], [4]. Moreover, since the decision boundary of SVM is solely defined by a few support vectors, the algorithm can tolerate random feature distortions and perturbations.

However, in many real applications, anomalous measurements are inherent to data set due to the strong environmental noise or the possible sensor failures. Examples include: industrial process monitoring, outdoor video surveillance, tactical multi-modal sensing, and, more generally, any application that involves unattended sensors in difficult environments. See, e.g., Fig. 1. Generally speaking, anomalous measurements are understood to be observations that have been corrupted, incorrectly measured, mis-recorded, drawn from different environments than those intended, or occurring too rarely to be useful in training a classifier [5]. If not robustified to anomalous measurements, classification algorithms may suffer from severe degradation of performance. Therefore, it is crucial

Tianpei Xie is with the Department of Electrical and Computer Engineering, University of Michigan, Ann Arbor, MI, 48109, USA e-mail: (tianpei@umich.edu).

Nasser M. Nasrabadi is with U.S. Army Research Lab., 2800 Powder Mill Road, Adelphi, MD, USA e-mail: (nasser.m.nasrabadi.civ@mail.mil)

Alfred O. Hero is with the Department of Electrical and Computer Engineering, University of Michigan, Ann Arbor, MI, 48109, USA e-mail: (hero@umich.edu).

to design robustness to anomalous data in order to reliably perform classification. This paper provides a new approach to perform robust large margin classification when training data is possibly corrupted by sensor failure.

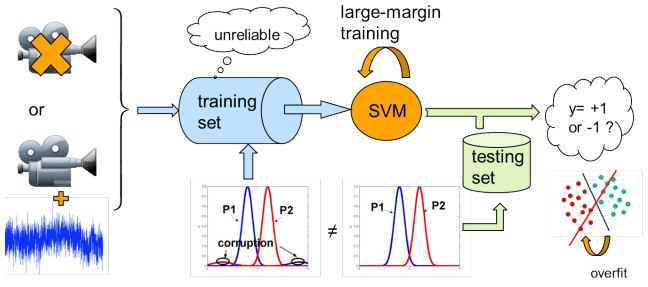


Fig. 1. Due to the corruption in training data set, the sample distributions of training and testing are different from each other, which makes decision boundary deviate from the normal direction.

## A. Problem settings and our contributions

To illustrate our setting, we divide the class of supervised training methods into four categories, according to the anomalous information available in different stages of a learning algorithm. It is summarized in Table I.

TABLE I  
CATEGORIES FOR SUPERVISED TRAINING ALGORITHMS VIA DIFFERENT ASSUMPTION OF ANOMALIES

	Training set (nominal)	Training set (corrupted)
Test set (nominal)	classical learning algorithms (e.g. SVM [6], MED [2] etc.)	Robust classification & training (e.g. ROD [7], <b>our work</b> etc.)
Test set (corrupted)	anomaly detection (e.g. MV [8], and GEM [9], [10] etc.)	Domain adaptation (e.g. [11] etc.)

As shown in Table I, a vast majority of learning algorithms assume that the training and test samples follow the same distribution and are both *nominal*; i.e., without anomalies. Under this assumption, an empirical error minimization algorithm is reasonable to achieve good performance in test set. If otherwise, anomalies exist in test data only, one refer to the anomaly detection algorithms, e.g. [8]–[10], [12], in which the main task is to classify anomalous samples from nominal ones. Under additional assumptions on nominal set, these algorithms can effectively identify an anomalous sample under given false alarm rate and missing probability. Furthermore, if both training and test set are corrupted but with different corruption rate, e.g. [11], [13], domain adaptation methods may apply, where the similarity between training and test distributions is explored to boost algorithm performance on test set.

Our work falls into the category of *robust classification & training* in which possibly anomalous samples may reside in

the training set while the test set is nominal. As mentioned above, in one aspect, the problem is motivated by many practical applications in which the quality of original data source is not of fully control. It thus of great interest for many practitioners to design a robust classification & training algorithm in their own area. On the other hand, however, providing a general framework is difficult from a theoretical perspective, since there is no reliable unbiased model available without specifying the intrinsic uncertainty in the dataset. As a result, the setting for robust classification & training reflects the interest of both practitioners and theorists and furthermore, it is considered as a tradeoff between them, under which a feasible solution is allowed to exist in both practice and theory.

In theoretical literature, the concept of robust estimation and classification has been thoroughly investigated [3], [4], [14]–[18]. In practice, however, only a few practical methods are available. For instance, the Ramp-Loss based SVM training methods have been studied in [3], [7], [19], [20]. Among them, Xu et al. [7] proposed the Robust-Outlier-Detection (ROD) by formulating outlier detection and removal directly in the standard soft margin framework. The resulting model is then solved via semi-definite programming (SDP). In one perspective, the models above are all non-convex in essence. This is due to the incompatibility between the convexity and outlier robustness inherited in the model assumption [5], [18]. In other perspective, from Table I, one can view, however, this problem as a *continuum* between a convex supervised learning problem and a nonconvex anomaly detection problem. Following this perspective, in this paper, we introduce a unified *convex* framework for robust classification so that both ends of this continuum are reached in a reliable way.

In specific, our proposed algorithm is motivated by the basic principle underlying the so-called *minimal volume (MV) /minimal entropy (ME) set anomaly detection methods* [6], [8]–[10]. Such techniques are expressly designed to detect anomalies in order to attain the lowest possible false alarm and miss probabilities and they are widely used during the training stage of algorithms. Moreover, since these methods are non-parametric and do not make explicit assumptions regarding the underling distribution, they are well-suited for our setting. Note that anomalous training samples will introduce global bias to a parametric model, whereas the bias is local for a non-parametric one. Among these methods, in particular, we focus on the Geometric Entropy Minimization (GEM) algorithm developed by Hero et al. etc [9], [10]. It estimates the ME set based on the k-nearest neighbor graph (k-NNG), which is shown to be the Uniformly Most Powerful Test at given level when the anomalies are drawn from an unknown mixture of known nominal density and uniform anomalous density [9]. A *key contributions* of this paper is the incorporation of the non-parametric GEM anomaly detection into a large margin classifier under a non-parametric corrupt-data model.

Finally, the proposed framework, namely, the *Geometric-Entropy-Minimization regularized Maximum Entropy Discrimination (GEM-MED)*, follows a *Bayesian* perspective. It is an extension of the well-established Maximum Entropy Dis-

crimination (MED) approach proposed by Jaakkola et al. [2]. MED performs Bayesian large margin classification via the maximum entropy principle and it subsumes SVM as a special case. It also provides a powerful framework that allow to be extended to parametric anomaly detection [2] and multitask classification [21]. However, the usage of MED in robust classification remained an open question before. In this paper, we answer this question confirmly using the GEM-MED model. In particular, the GEM-MED can effectively minimize the generalization error under the nominal distribution and can distinguish the sensor failures from nominal samples under a prescribed threshold on false alarm rate. We demonstrate its superior performance over other outlier-resistant classifier learning methods on simulated data and on a real data set, containing human and human-leading-animal footsteps, collected in the field by a set of acoustic sensors [22]–[24].

### B. Organization of the paper

What follows is a brief outline of the paper: In Section **II**, we introduce the MED as a general framework that both fits into the convention classification and the anomaly detection setting. A natural transition from MED to a robustified MED is then followed, with the GEM-MED framework considered as a modification of the framework, when the score function is approximated via the Geometric-Entropy-Minimization (GEM) technique. Both the GEM principle and the GEM-MED approach are presented In Section **III**. We then proposed a solution using variational inference in Section **IV**. The experimental results based on synthesis data and real data are presented in Section **V**.

## II. FROM MED TO GEM-MED: A GENERAL ROUTINE

Denote the training data set as  $\mathcal{D}_t \equiv \{(y_n, \mathbf{x}_n)\}_{n \in T}$ , where each sample-pair  $(y_n, \mathbf{x}_n) \in \mathcal{Y} \times \mathcal{X} \equiv \mathcal{D}$  are independent. For simplicity, assume that  $\mathcal{X} \subset \mathbb{R}^p$ ,  $\mathcal{Y} = \{-1, 1\}$ . The test data set is denoted as  $\mathcal{D}_s \equiv \{\mathbf{x}_m\}_{m \in S}$ . Moreover, assume that  $(y_n, \mathbf{x}_n) \sim \mathcal{P}_t$  is the underlying distribution for training data and  $\mathcal{P}_s$  is the distribution for test samples. Let  $\mathcal{P}_{nom}$  be the nominal distribution.

### A. Maximum entropy discrimination (MED)

First, consider the conventional setting as  $\mathcal{P}_t = \mathcal{P}_s = \mathcal{P}_{nom}$ . Many learning algorithms under this setting can be formulated as minimizing a model complexity term under a set of error constraints as

$$\mathcal{L}_C(f, (y_n, \mathbf{x}_n); \Theta) \leq \xi_n, \quad n \in T, \quad (1)$$

where  $f : \mathcal{X} \rightarrow \mathcal{Y}$  is the unknown classifier which by assumption lies in  $\mathcal{H}$ , the space of classification functions of interest,  $\xi_n \geq 0$  for all  $n \in T$  is the slack variables that guarantee nonempty feasible region. The error functional  $\mathcal{L}_C : \mathcal{H} \times \mathcal{D} \rightarrow \mathbb{R}_+$  in (1) could be modeled as

$$\mathcal{L}_C(f, (y_n, \mathbf{x}_n); \Theta) = \text{e.g. } \begin{cases} \log(1 + \exp(-y_n f(\mathbf{x}_n; \Theta))) & \text{logistic regression} \\ \exp(-y_n f(\mathbf{x}_n; \Theta)) & \text{Adaboost} \\ [\rho - y_n f(\mathbf{x}_n; \Theta)]_+ & \text{SVM}, \end{cases}$$

where  $[\cdot] = \max\{0, \cdot\}$ . Here  $\Theta$  provide a parameterization of function  $f(\cdot) \equiv f(\cdot; \Theta)$  which is learned from the algorithm.

The conventional framework, however, does not fit into the robust learning setting, where  $\mathcal{P}_t \neq \mathcal{P}_s$  with  $\mathcal{P}_s = \mathcal{P}_{nom}$ . There are two difficulties: first, the deterministic function  $f$  does not model the uncertainty in decision explicitly. It is especially important since the possibly anomalous training samples will generate unreliable classifiers; second, the error functional  $\mathcal{L}_C$  as predefined above lacks of proper flexibility in modeling.

The Maximum entropy discrimination (MED) proposed by Jaakkola et al [2] overcomes these issues by considering a generative model  $p(y, \mathbf{x}; \Theta) \in \Delta_{\mathcal{Y} \times \mathcal{X}}$  with random parameter  $\Theta \sim q(\Theta)$ , where  $\Delta_{\mathcal{Y} \times \mathcal{X}}$  is the probability simplex on  $\mathcal{D} \equiv \mathcal{Y} \times \mathcal{X}$ . Moreover, the error constraints is modeled as a convex combination of error functionals; i.e.,

$$\int q(\Theta) \mathcal{L}_C(p, (y_n, \mathbf{x}_n); \Theta) d\Theta \leq \xi_n, \quad n \in T, \quad (2)$$

with the error functional  $\mathcal{L}_C : \Delta_{\mathcal{Y} \times \mathcal{X}} \times \mathcal{D} \rightarrow \mathbb{R}_+$  defined as

$$\begin{aligned} \mathcal{L}_C(p, (y_n, \mathbf{x}_n); \Theta) \\ = \text{e.g. } \begin{cases} \log \{p(y = y_n, \mathbf{x}_n; \Theta) / p(y \neq y_n, \mathbf{x}_n; \Theta)\}, & \text{log-odds;} \\ [\rho - \log \{p(y = y_n, \mathbf{x}_n; \Theta) / p(y \neq y_n, \mathbf{x}_n; \Theta)\}]_+, & \text{max-margin.} \end{cases} \end{aligned}$$

For instance, if  $p$  is the Gaussian mixture models with common covariance,  $p(y, \mathbf{x}; \Theta) = \sum_{z \in \{\pm 1\}} \mathbb{1}\{y = z\} \mathcal{N}(\mathbf{x} | \mathbf{m}_z, \Sigma)$ , where  $\Theta = (\mathbf{m}_{-1}, \mathbf{m}_1, \Sigma)$ , then the log-odds classifier in (2) is a linear constraint with respect to (w.r.t.)  $(y, \mathbf{x})$ .

Following the Bayesian perspective, the goal of MED is to learn a posterior distribution  $q(\Theta) \in \Delta_\Theta$  given a prior distribution  $p_0(\Theta)$ ; in particular, it is formulated as following problem

$$\begin{aligned} \min_{q(\Theta) \in \Delta_\Theta, \xi} \quad & \text{KL}(q(\Theta) \| p_0(\Theta)) + \sum_{n \in T} \xi_n \\ \text{s.t.} \quad & \int q(\Theta) \mathcal{L}_C(p, (y_n, \mathbf{x}_n); \Theta) d\Theta \leq \xi_n, \quad n \in T, \\ & \xi_n \geq 0, \quad n \in T, \end{aligned} \quad (3)$$

where  $\text{KL}(q \| p) = \mathbb{E}_q \left[ \log \left( \frac{p}{q} \right) \right]$  is the KL-divergence and  $\xi_n \geq 0$  for all  $n \in T$  is the slack variables as defined before. As shown in [2], the problem (3) is convex and it is viewed as a projection of prior distribution  $p_0(\Theta)$  into a feasible region defined by error constraints (2). In [21], [25], with specific domain knowledge incorporated, MED achieves the superior performance among many other learning algorithms.

Note that if the prior is a Gaussian process  $p_0(\Theta) \equiv p_0(f) = \mathcal{N}(\mathbf{0}, K)$  on the parametric random functions  $f : \mathcal{X} \rightarrow \mathcal{Y}$  with  $f(\cdot) \equiv f(\cdot; \Theta) \in \mathcal{H}$ , and  $\mathcal{H}$  is a Reproducing Kernel Hilbert Space (RKHS) associated with kernel  $K$ , then the MED model is readily to handle the nonlinear features as in the case of SVM. See [21] for more detailed discussion.

In testing phase, the prediction is based on the averaged

score generated by multiple log-likelihood functionals; i.e.,

$$y^* = \operatorname{argmin}_y \left\{ - \int q(\Theta) \log p(y, \mathbf{x}_m; \Theta) d\Theta \right\}, \quad \mathbf{x}_m \in \mathcal{D}_s. \quad (4)$$

### B. MED for anomaly detection

The soft-constraint framework in (3) allows the MED to perform anomaly detection under the setting  $\mathcal{P}_t \neq \mathcal{P}_s$ , but  $\mathcal{P}_t = \mathcal{P}_{nom}$ . In specific, given the log-likelihood  $\log p(\mathbf{x}; \Theta)$ , the *rejection region* for the anomaly test is  $\Psi_\beta \equiv \{\mathbf{x}_m \in \mathcal{X} \mid \log p(\mathbf{x}_m; \Theta) \geq \beta\}$ . Here,  $\Psi_\beta$  is a  $\beta$ -level-set region for a given model  $p(\mathbf{x}; \Theta)$ . Then the test strategy is to declare  $\mathbf{x}_m \in \mathcal{D}_s$  as anomalous whenever  $\mathbf{x}_m \notin \Psi_\beta$ ; and declare it as nominal if  $\mathbf{x}_m \in \Psi_\beta$ . Intuitively, it follows from the fact the anomalies such as sensor failures are assumed to be rare events. The above test strategy can be formulated as a constraint

$$\int q(\bar{\Theta}) \mathcal{L}_D(p, \mathbf{x}_n; \bar{\Theta}) d\bar{\Theta} \geq 0, \quad n \in T, \quad (5)$$

where the test functional  $\mathcal{L}_D : \Delta_{\mathcal{X}} \times \mathcal{X} \rightarrow \mathbb{R}_+$  is defined as

$$\mathcal{L}_D(p, \mathbf{x}_n; \bar{\Theta}) = [\log p(\mathbf{x}_n; \Theta) - \beta]$$

with  $\bar{\Theta} = \Theta \cup \{\beta\}$  and  $q(\bar{\Theta}) = q(\Theta, \beta)$ .

By replacing (2) in (3) with (5), a parametric estimation  $\hat{\Psi}_\beta$  of  $\Psi_\beta$  is obtained via MED by finding an optimal threshold  $\hat{\beta} > 0$  that is compatible with a learned distribution parameter  $\hat{\Theta}$  so that all training samples in  $\mathcal{D}_t \subset \hat{\Psi}_\beta$ , by  $\mathcal{P}_t = \mathcal{P}_{norm}$ . In specific, if the marginal model  $p(\mathbf{x}; \hat{\Theta}) = \mathcal{P}_{norm}$ , then this approach will guarantee that the false alarm rate of the test is bounded above.

In summary, MED provide a framework that naturally fit into the conventional classification setting, where  $\mathcal{P}_t = \mathcal{P}_s = \mathcal{P}_{nom}$ , and the anomaly detection setting, where  $\mathcal{P}_t \neq \mathcal{P}_s$ , and  $\mathcal{P}_t = \mathcal{P}_{nom}$ . This makes it a strong candidate for robust classification, where  $\mathcal{P}_t \neq \mathcal{P}_s$  with  $\mathcal{P}_s = \mathcal{P}_{nom}$ . However, as will be shown later, a straightforward robustified MED model is not readily to use without proper modification.

### C. MED in robust classification

In ideal situations, one can perform robust classification via both conventional classification and anomaly detection: assume a partition of training samples  $\mathcal{D}_t = \mathcal{D}_t^{nom} \cup \mathcal{D}_t^{anm}$ , where  $(\mathbf{x}_n, y_n) \sim \mathcal{P}_{nom}$  if  $(\mathbf{x}_n, y_n) \in \mathcal{D}_t^{nom}$  and  $(\mathbf{x}_n, y_n) \not\sim \mathcal{P}_{nom}$ , if  $(\mathbf{x}_n, y_n) \in \mathcal{D}_t^{anm}$ . Clearly, the pair  $(\mathcal{D}_t^{nom}, \mathcal{D}_s)$  follows a conventional classification setting with the pair  $(\mathcal{D}_t^{nom}, \mathcal{D}_t^{anm})$  under the anomaly detection setting. Following this perspective, the MED for robust classification is simply given by

$$\begin{aligned} \min_{q(\bar{\Theta}) \in \Delta_{\bar{\Theta}}} \quad & \text{KL}(q(\bar{\Theta}) \| p_0(\bar{\Theta})) \\ \text{s.t.} \quad & \int q(\bar{\Theta}) \mathcal{L}_C(p, (y_n, \mathbf{x}_n); \bar{\Theta}) d\bar{\Theta} \leq 0, \quad (\mathbf{x}_n, y_n) \in \mathcal{D}_t^{nom}, \\ & \int q(\bar{\Theta}) \mathcal{L}_D(p, \mathbf{x}_n; \bar{\Theta}) d\bar{\Theta} \geq 0, \quad (\mathbf{x}_n, y_n) \in \mathcal{D}_t^{anm}, \end{aligned} \quad (6)$$

where  $\overline{\Theta} = \Theta \cup \{\beta\} \cup \{\xi_n, n \in T\}$  with error functional  $\mathcal{L}_C$  and test functional  $\mathcal{L}_D$  defined as

$$\begin{aligned}\mathcal{L}_C(p, (y_n, \mathbf{x}_n); \overline{\Theta}) \\ = \xi_n - \log \{p(y = y_n, \mathbf{x}_n; \Theta)/p(y \neq y_n, \mathbf{x}_n; \Theta)\} \quad (7) \\ \mathcal{L}_D(p, \mathbf{x}_n; \overline{\Theta}) = [\log p(\mathbf{x}_n; \Theta) - \beta].\end{aligned}$$

See that (7) is a large-margin functional as in SVM.

Unfortunately, there are several critical problems, which prevents its usage in practice:

- 1) The partition  $\mathcal{D}_t = \mathcal{D}_t^{nom} \cup \mathcal{D}_t^{anm}$  is not available beforehand. Note that finding  $\mathcal{D}_t^{nom}$  is equivalent as finding a parametric estimation of level-set region  $\Psi_\beta \equiv \{\mathbf{x}_m \in \mathcal{X} \mid \log p(\mathbf{x}_m; \Theta) \geq \beta\}$  given all the training samples  $\mathcal{D}_t$  with anomalies included. The method in (5), e.g., does not fit into this situation.
- 2) Training samples in  $\mathcal{D}_t^{anm} = \mathcal{D}_t \setminus \mathcal{D}_t^{nom}$  does not contribute to the learning algorithm, even though many of them may follow a distribution that is close to the nominal one. This limited-training-set problem is especially severe, if the partition  $\mathcal{D}_t^{nom}$  is estimated by an over-permissive estimator, which will cause unnecessary performance degradation due to lack of training samples.
- 3) Utilizing inaccurate parametric model  $p(y, x; \Theta)$  in defining  $\Psi_\beta$  will introduce an additional bias into the learning algorithm. As a result, whenever  $\mathcal{P}_{nom} \notin \{p(y, x; \Theta); \Theta \in \mathcal{T}\}$ , there is no theoretical guarantee on the false alarm rate and missing probability.

To solve these problems, we

- 1) find an alternative rejection region that is feasible under the above setting utilizing the minimal-entropy-set [9].
- 2) apply an unnormalized weight for each sample to reuse a portion of data out of rejection region.
- 3) use a non-parametric estimator to find the rejection region. The resulting estimator is built upon a non-parametric estimation of true underlying distribution of data, with a theoretical guarantee on the false alarm rate and missing probability provided.

### III. THE GEM-MED: MODEL FORMULATION

#### A. Anomaly detection using minimal-entropy set

Instead of finding the level-set region  $\Psi_\beta \equiv \{\mathbf{x}_m \in \mathcal{X} \mid \log p(\mathbf{x}_m; \Theta) \geq \beta\}$ , we resort to the *minimal-entropy (ME) set*  $\Omega_{1-\beta}$  as an alternative. In particular,  $\Omega_{1-\beta} \equiv \arg \min_A \{H(A) : \int_A p(\mathbf{x}) d\mathbf{x} \geq \beta\}$  is referred as the *minimal-entropy-set of false alarm level*  $1 - \beta$ , where  $H(A) = -\int_A \log p(\mathbf{x}) p(\mathbf{x}) d\mathbf{x}$  is the Shannon entropy of the density  $p(\mathbf{x})$  over the region  $A$ . This minimal-entropy-set is defined upon the *epigraph-set*  $\{A : \int_A p(\mathbf{x}) d\mathbf{x} \geq \beta\}$ . In Fig. 2, we show an illustrative example of epigraph-set and compare it with the level-set  $\Psi_\beta$ .

Note that the low entropy region corresponds to the high density region. Following the same principle as in (5), the

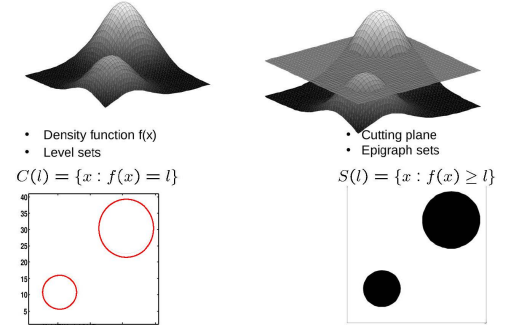


Fig. 2. The comparison of level-set (left) and the epigraph-set (right) w.r.t. the common distribution function. The minimum-entropy-set is computed based on the epigraph-set.

local entropy  $-\mathbb{E}_p [\log p(x)]$  can serve as an alternative test statistics in anomaly detection. In particular, given  $\Omega_{1-\beta}$ , a sample  $\mathbf{x}_n$  is declared anomalous if  $\mathbf{x}_n \notin \Omega_{1-\beta}$ ; and it is declared nominal, when  $\mathbf{x}_n \in \Omega_{1-\beta}$ . It is proved in [9] that this test is a Uniformly Most Powerful Test (UMPT) at level  $\beta$  when the anomalies are drawn from an unknown mixture of known nominal density  $p(\mathbf{x})$  and uniform anomalous density.

A benefit for using ME set as a rejection region is that efficient approximation algorithms are available without knowing the true training data distribution  $\mathcal{P}_t$  in advance. In particular, the Geometric Entropy Minimization (GEM) proposed by Hero et al. [9], [10] approximates the ME set by replacing  $\Omega_{1-\beta}$  with an empirical estimate  $\hat{\Omega}_{1-\beta}$  using a non-parametric estimation of underlying empirical distribution  $\hat{\mathcal{P}}_t$ . The detail in implementation is discussed later in Section III-C.

#### B. The GEM-MED as non-parametric robustified MED

Given the notion of ME set  $\Omega_{1-\beta}$ , we now modify the framework in (6). First, we associate each training sample  $\mathbf{x}_n \in \mathcal{D}_t$  with a unnormalized weight  $\eta_n \in [0, 1]$ . Each weight  $\eta_n$  is the indicator function of the event  $\mathbf{x}_n \in \Omega_{1-\beta}$ , and denote the rejection region  $\mathcal{D}_t^{nom}(\boldsymbol{\eta}) \equiv \{\mathbf{x}_n : \eta_n > 0\} = \mathcal{D}_t \cap \Omega_{1-\beta}$ . The weight  $\{\eta_n, n \in T\}$  is approximated via solving  $\hat{\boldsymbol{\eta}} = \arg \min \{ \sum_n \eta_n \hat{h}_n / |T| : \sum_n \eta_n / |T| \geq \beta \}$ , where  $\hat{h}_n \equiv -\log \hat{p}(\mathbf{x}_n)$  is the empirical entropy estimated by GEM. Given all  $\hat{h}_n, n \in T$ , it is simply a linear optimization.

Now assume that  $\boldsymbol{\eta} \sim q(\boldsymbol{\eta})$  is random, we define the test functional  $\tilde{\mathcal{L}}_D$  as

$$\begin{aligned}\tilde{\mathcal{L}}_D(\boldsymbol{\eta}, \gamma_{-1}, \gamma_{+1}, \mathbf{y}; z, \hat{\mathbf{h}}) \\ = \left( \gamma_z - \sum_n \mathbf{1}\{\mathbf{y}_n = z\} \eta_n \hat{h}_n / |T| \right), \quad z \in \{\pm 1\}\end{aligned}$$

where  $\gamma_z \geq 0, z \in \{\pm 1\}$  is the threshold associated with the empirical entropy  $\hat{h}_n$  on  $\mathcal{D}_t \cap \{\mathbf{y}_n = z\}$ . Note that  $\tilde{\mathcal{L}}_D$  is linear w.r.t.  $(\boldsymbol{\eta}, \gamma_{-1}, \gamma_{+1})$ .

With the test functional  $\tilde{\mathcal{L}}_D$  defined, the test constraint

$$\int q(\overline{\Theta}) \mathcal{L}_D(p, \mathbf{x}_n; \overline{\Theta}) d\overline{\Theta} \geq 0, \quad (\mathbf{x}_n, y_n) \in \mathcal{D}_t^{nom}$$

in (6) is replaced by

$$\int q(\tilde{\Theta}) \tilde{\mathcal{L}}_D(\tilde{\Theta}, \mathbf{y}; z, \hat{\mathbf{h}}) d\tilde{\Theta} \geq 0, z = \pm 1, \quad (8)$$

$$\int q(\tilde{\Theta}) \left[ \sum_{n:y_n=z} \eta_n / |T| \right] d\tilde{\Theta} \geq \beta, z = \pm 1, \quad (9)$$

where  $\tilde{\Theta} = \Theta \cup \{\xi_n, n \in T\} \cup \eta \cup \{\gamma_{+1}, \gamma_{-1}\}$ . The constraint (8) is referred as *the entropy constraint* and constraint (9) is the *epigraph constraint*. Combining these constraints will give an approximation of  $\hat{\Omega}_{1-\beta} \cap \{\mathbf{x}_n : y_n = z\}, z = \pm 1$ .

Similarly, the error constraints

$$\int q(\bar{\Theta}) \mathcal{L}_C(p, (y_n, \mathbf{x}_n); \bar{\Theta}) d\bar{\Theta} \leq 0, (\mathbf{x}_n, y_n) \in \mathcal{D}_t^{nom},$$

in (6) is replaced by *reweighted* error constraints

$$\int q(\tilde{\Theta}) \left[ \eta_n \mathcal{L}_C(p, (y_n, \mathbf{x}_n); \tilde{\Theta}) \right] d\tilde{\Theta} \leq 0, n \in T,$$

with  $\mathcal{L}_C$  defined as in (7). Note that these constraints apply to all training data.

Now we have the following model:

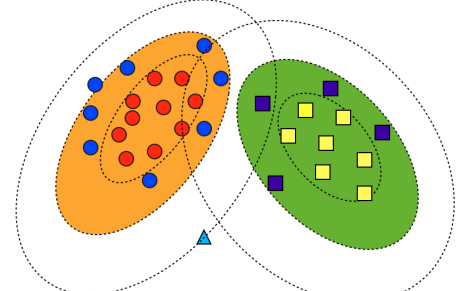
**Definition** The *Geometric-Entropy-Minimization Maximum-Entropy-Discrimination (GEM-MED)* model is presented as

$$\begin{aligned} \min_{q(\tilde{\Theta}) \in \Delta_{\tilde{\Theta}}} \quad & \text{KL} \left( q(\tilde{\Theta}) \parallel p_0(\tilde{\Theta}) \right) \\ \text{s.t.} \quad & \int q(\tilde{\Theta}) \left[ \eta_n \mathcal{L}_C(p, (y_n, \mathbf{x}_n); \tilde{\Theta}) \right] d\tilde{\Theta} \leq 0, n \in T, \\ & \int q(\tilde{\Theta}) \tilde{\mathcal{L}}_D(\tilde{\Theta}, \mathbf{y}; z, \hat{\mathbf{h}}) d\tilde{\Theta} \geq 0, z = \pm 1, \\ & \int q(\tilde{\Theta}) \left[ \sum_{n:y_n=z} \eta_n / |T| \right] d\tilde{\Theta} \geq \beta, z = \pm 1 \end{aligned} \quad (10)$$

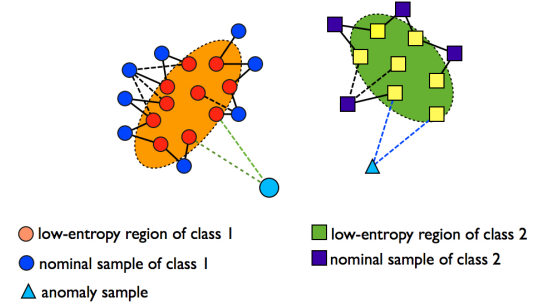
where  $\tilde{\Theta} = \Theta \cup \{\xi_n, n \in T\} \cup \eta \cup \{\gamma_{+1}, \gamma_{-1}\}$ ,  $\mathcal{L}_C$  is defined as in (7),  $\tilde{\mathcal{L}}_D$  is defined as in (8). Here,  $\eta_n \in [0, 1], n \in T$  is the unnormalized weight associated with each training sample  $\mathbf{x}_n \in \mathcal{D}_t$ . The  $\hat{\mathbf{h}} = (\hat{h}_n, n \in T)$  with  $\hat{h}_n \equiv -\log \hat{p}(\mathbf{x}_n)$  given by GEM.

### C. The non-parametric entropy estimation via GEM

In implementation of GEM, we utilize a *bipartite K-point k-nearest neighbor graph* (BP-kNNG) [10]. Specifically, we treat  $\mathcal{D}_t^c \equiv \{\mathbf{x}_n : y_n = c\}$  with each label  $c = \pm 1$  independently. Define a random partitioning  $\mathcal{D}_t^c = \mathcal{D}_t^{N,c} \cup \mathcal{D}_t^{M,c}$ . As shown in Fig. 3, the BP-kNNG is built as a set of edges connecting these two parts, in which one part is used to estimate the entropy functional form  $\hat{h}(\cdot) = -\log(\hat{p}(\cdot))$ , while the other part to compute the average entropy within a neighborhood. In particular, for  $\mathbf{x}_n \in \mathcal{D}_t^{N,c}$ , the entropy  $\hat{h}_n$  is estimated via  $-\log(\hat{p}(\mathbf{x}_n)) = d \log(R_k(\mathbf{x}_n)) - \log \left( \frac{k-1}{M_c c_d} \right)$ , where  $R_k(\mathbf{x}_n)$  is the sum of k-nearest neighbor (kNN) distance from the target sample  $\mathbf{x}_n$  to its  $M_c$  reference samples in  $\mathcal{D}_t^{M,c}$ ;  $d$  is the intrinsic dimension of  $\mathbf{x}_n$  and  $c_d$  is the volume of the unit ball in  $d$  dimensions. See [10] for further proof and details.



(a)



(b)

Fig. 3. The illustration of minimum-entropy-set (a), estimated using a bipartite K-point k-nearest neighbor graph (BP-kNNG) (b) for each class in the training set. Note that the average kNN distance for anomalies should be significantly larger than the nominal samples, due to its local entropy property.

## IV. ALGORITHM

### A. Solving (10) via projected stochastic gradient descent algorithm

To solve the GEM-MED model, it is seen that the problem in (10) is convex w.r.t. the unknown distribution  $q(\tilde{\Theta})$ . Therefore, solving a system of equations via KKT condition will result in the unique optimal solution.

In particular, we have the following result:

**Proposition 4.1:** The GEM-MED problem in (10) is convex with respect to the unknown distribution  $q(\tilde{\Theta})$  and the unique optimal solution is given as a generalized Gibbs distribution:

$$q(\tilde{\Theta}) = \frac{1}{Z(\boldsymbol{\lambda}, \boldsymbol{\mu}, \boldsymbol{\kappa})} p_0(\tilde{\Theta}) \exp \left( -E(\tilde{\Theta}; \boldsymbol{\lambda}, \boldsymbol{\mu}, \boldsymbol{\kappa}) \right), \quad (11)$$

$$\begin{aligned} \text{where } E(\tilde{\Theta}; \boldsymbol{\lambda}, \boldsymbol{\mu}, \boldsymbol{\kappa}) = & \sum_{n \in T} \lambda_n \eta_n \mathcal{L}_C - \sum_{z \in \{\pm 1\}} \mu_z \tilde{\mathcal{L}}_{D,z} \\ & - \sum_{z \in \{\pm 1\}} \kappa_z \sum_{n:y_n=z} \eta_n / |T| + \sum_{z \in \{\pm 1\}} \kappa_z \beta \end{aligned}$$

and the dual variables  $\boldsymbol{\lambda} = \{\lambda_n, n \in T\} \succeq \mathbf{0}$ ,  $\boldsymbol{\mu} = (\mu_z, z \in \{\pm 1\}) \succeq \mathbf{0}$  and  $\boldsymbol{\kappa} = (\kappa_z, z \in \{\pm 1\}) \geq \mathbf{0}$ .  $Z(\boldsymbol{\lambda}, \boldsymbol{\mu}, \boldsymbol{\kappa})$  is the partition function, which is given as

$$Z(\boldsymbol{\lambda}, \boldsymbol{\mu}, \boldsymbol{\kappa}) = \int p_0(\tilde{\Theta}) \exp \left( -E(\tilde{\Theta}; \boldsymbol{\lambda}, \boldsymbol{\mu}, \boldsymbol{\kappa}) \right) d\tilde{\Theta}. \quad (12)$$

The factor  $\mathcal{L}_C$  is defined as in (7),  $\tilde{\mathcal{L}}_{D,z} \equiv \tilde{\mathcal{L}}_D(\cdot; z, \cdot)$  is defined as in (8).

See the appendix A for a brief proof. ■

To simplify the expression (11) and (12), we make following assumptions:

1) Define the decision function  $f : \mathcal{X} \rightarrow \mathcal{Y}$  as

$$f(\mathbf{x}_n) = y_n \log \{p(y = y_n, \mathbf{x}_n; \Theta)/p(y \neq y_n, \mathbf{x}_n; \Theta)\}$$

with  $\{\mathbf{x} : f(\mathbf{x}) = 0\}$  being the decision boundary. Therefore, the error functional is redefined as

$$\mathcal{L}_C(f, (y_n, \mathbf{x}_n); (\tilde{\Theta}/\Theta)) = \xi_n - y_n f(\mathbf{x}_n) \quad (13)$$

2) Assume the prior

$$p_0(\tilde{\Theta}) = p_0(\Theta) \prod_{n \in T} p_0(\xi_n) \prod_{n \in T} p_0(\eta_n) \prod_{z \in \{\pm 1\}} p_0(\gamma_z) \quad (14)$$

is fully factorized.

3) Assume that  $f$  is random and replace  $\Theta$  with  $f$ . Also assume the Gaussian process as the prior for random function  $f$ ; in specific,

$$\begin{aligned} p_0(\Theta) &\equiv p_0(f) = \mathcal{N}(0, K), \\ p_0(f | \mathcal{D}_t) &= \mathcal{N}(\mathbf{0}, \mathbf{K}), \end{aligned} \quad (15)$$

where  $\text{cov}(f(\mathbf{x}_i), f(\mathbf{x}_j)) \equiv K(\mathbf{x}_i, \mathbf{x}_j)$ ,  $K : \mathcal{X} \times \mathcal{X} \rightarrow \mathbb{R}$  is covariance kernel function,  $\mathbf{K} = [K(\mathbf{x}_i, \mathbf{x}_j)]_{i,j \in T}$ . Also

$$q(\Theta | \mathcal{D}_t) \equiv q(f | \mathcal{D}_t)$$

4) Assume that

$$\begin{aligned} p_0(\xi_n) &\propto \exp(-c_\xi(1 - \xi_n)), \quad \xi_n \in (-\infty, 1], \quad n \in T; \\ p_0(\eta_n) &= \text{Ber}(p_\eta) \\ \text{with } p_\eta &= \frac{1}{1 + \exp(-(a_\eta - \eta_n))} \\ &\equiv \sigma(a_\eta - \eta_n), \quad \eta_n \in \{0, 1\}, \quad n \in T; \\ p_0(\gamma_z) &= \delta_{\hat{\gamma}_z}(\gamma_z); \quad z \in \{\pm 1\}, \end{aligned} \quad (16)$$

where  $(a_\eta, c_\xi)$  are hyperparameter and  $\hat{\gamma}_z$  is the upper bound estimate for K-point minimal-entropy in each class  $z = \pm 1$  given by GEM algorithm.  $\sigma(x) = 1/(1 + \exp(-x))$  is the sigmoid function.

With all these assumptions, the following result is available:

**Proposition 4.2:** Under the factorized prior (14), with assumption in (13), (15), (16), the dual optimization problem is given as

$$\begin{aligned} &\max_{\lambda, \mu, \kappa \geq 0} -\log Z(\lambda, \mu, \kappa) \quad (17) \\ &= -\log \int p_0(\tilde{\Theta}) \exp \left( -E(\tilde{\Theta}; \lambda, \mu, \kappa) \right) d\tilde{\Theta} \\ &= \sum_{n \in T} (\lambda_n + \log(1 - \lambda_n/c)) - \sum_{z \in \{\pm 1\}} \mu_z \hat{\gamma}_z + (\sum \kappa_z) \beta \\ &\quad - \log \int \exp \left( \frac{1}{2} Q(\mathbf{K} \odot (\mathbf{y}\mathbf{y}^T), (\lambda \odot \eta)) \right) \end{aligned}$$

$$\times p_0(\eta) \exp \left( +\eta^T (-\mu \otimes \hat{\mathbf{h}} + \kappa \otimes \mathbf{e}) \right) d\eta \quad (18)$$

where  $\mathbf{e}$  is a all 1's vector,  $\odot$  is pointwise product,  $\otimes$  is the kronecker product, respectively, and

$$Q(\mathbf{K}, \mathbf{x}) = \mathbf{x}^T \mathbf{K} \mathbf{x}$$

is the quadratic form associated with the kernel  $K$ .

See Appendix B for derivations. ■

It is seen from (17) that the dual objective function is concave w.r.t. dual variables  $(\lambda, \mu, \kappa)$ . However, the expression in (18) cannot be integrated out, so an explicit form as a quadratic optimization in SVM is not available. Nevertheless, the only coupling in (18) comes from the joint distribution  $q(f, \eta)$ . In particular, we have the following

**Proposition 4.3:** For the optimal solution (11) under the prior assumption (14), (13), (15) and (16), the following holds

- 1)  $q(\tilde{\Theta}) = q(f, \eta) \prod_n q(\eta_n)$  is factorized.
- 2)  $q(\eta | f) = \prod_{n \in T} q(\eta_n | f)$ , i.e. the  $\{\eta_n, n \in T\}$  are conditional independent given the decision boundary function  $f$ . In particular,

$$\begin{aligned} q(\eta_n | f) &= \text{Ber}(q_\eta), \quad (19) \\ \text{with } q_\eta &= \sigma(\rho_n \mathcal{F}_n(f)) \end{aligned}$$

$$\text{where } \rho_n \equiv \log \frac{1 - p_0(\eta_n = 1)}{p_0(\eta_n = 1)}, \quad \mathcal{F}_n(f) \equiv \lambda_n [y_n f(\mathbf{x}_n) - 1] - \mu_{y_n} h_n + \kappa_{y_n} / \|T\|.$$

- 3)  $q(f | \eta) = \mathcal{N}(\hat{f}_{\eta, \lambda}(\cdot) | \mathbf{K})$ , where

$$\hat{f}_{\eta, \lambda}(\cdot) = \sum_{n \in T} \lambda_n \eta_n y_n K(\cdot, \mathbf{x}_n) \in \mathcal{H} \quad (20)$$

See proof in Appendix C. ■

Given **Proposition 4.2** and **Proposition 4.3**, we propose to use the *projected stochastic gradient descent* (i.e. PSGD, [26]) algorithm to solve the dual optimization problem in (18).

In specific, the gradient vectors of the dual objective function in (18) w.r.t.  $\lambda, \mu, \kappa$ , respectively, are computed as

$$\begin{aligned} &\frac{\partial}{\partial \lambda_n} [-\log Z(\lambda, \mu, \kappa)] \\ &= 1 - \mathbb{E}_{q(f, \eta)} [\eta_n y_n f(\mathbf{x}_n)] + \frac{c}{c - \lambda_n}, \quad n \in T; \end{aligned} \quad (21)$$

$$\begin{aligned} &\frac{\partial}{\partial \mu_z} [-\log Z(\lambda, \mu, \kappa)] \\ &= \mathbb{E}_{q(f, \eta)} \left\{ \sum_{n: y_n = z} \eta_n h_n \right\} - \hat{\gamma}_z, \quad z = \pm 1; \end{aligned} \quad (22)$$

$$\begin{aligned} &\frac{\partial}{\partial \kappa_z} [-\log Z(\lambda, \mu, \kappa)] \\ &= \beta - \frac{1}{|T|} \mathbb{E}_{q(f, \eta)} \left[ \sum_{n: y_n = z} \eta_n \right], \quad z = -1, +1. \end{aligned} \quad (23)$$

Note that the expectation w.r.t.  $q(f, \eta)$  are approximated by Gibbs sampling with each conditional distribution given as Lemma 4.3.

---

**Algorithm 1** The (kernel) GEM-MED algorithm

---

**Input:** The training set  $\mathcal{D}_t \subset \mathcal{X} \times \{\pm 1\}$  and the test set  $\mathcal{D}_s$ . Prior distribution and assumptions given as (13)-(16). The kernel function  $K : \mathcal{X} \times \mathcal{X} \rightarrow \mathbb{R}$ .

1: **Initialize:** Set  $\boldsymbol{\mu}_0 = \mathbf{0}, \boldsymbol{\kappa}_0 = \mathbf{0}, \boldsymbol{\lambda}_0$  is set by applying conventional MED on  $\mathcal{D}$

2: **for**  $t = 1, \dots, T$  or until converge **do**

3: Compute the gradient of log-partition function w.r.t  $\boldsymbol{\lambda}_t, \boldsymbol{\mu}_t$  and  $\boldsymbol{\kappa}_t$ , respectively, i.e.  $\frac{\partial \log Z(\boldsymbol{\lambda}_t, \boldsymbol{\mu}_t, \boldsymbol{\kappa}_t)}{\partial \lambda_n}$ ,  $\frac{\partial \log Z(\boldsymbol{\lambda}_t, \boldsymbol{\mu}_t, \boldsymbol{\kappa}_t)}{\partial \mu_z}$  and  $\frac{\partial \log Z(\boldsymbol{\lambda}_t, \boldsymbol{\mu}_t, \boldsymbol{\kappa}_t)}{\partial \kappa_z}$  according to the formula (21)-(23) where the expectation is approximated via Gibbs sampling described as above.

4: Update  $\lambda_n, \mu_z$  and  $\kappa_z$  via projected gradient descent, i.e.

$$\begin{aligned}\lambda_{n,(t+1)} &= \text{proj}_{\{\lambda: 0 \leq \lambda \leq C_1\}} \left\{ \lambda_{n,t} - \varphi \frac{\partial \log Z((\boldsymbol{\mu}_t, \boldsymbol{\lambda}_t, \boldsymbol{\kappa}_t))}{\partial \lambda_n} \right\} \\ &\quad n \in T, \\ \mu_{z,(t+1)} &= \text{proj}_{\{\mu: \mu \geq 0\}} \left\{ \mu_{z,t} - \psi \frac{\partial \log Z(\boldsymbol{\mu}_t, \boldsymbol{\lambda}_t, \boldsymbol{\kappa}_t)}{\partial \mu_z} \right\} \\ &\quad z \in \{-1, +1\}, \\ \kappa_{z,(t+1)} &= \text{proj}_{\{\kappa: \kappa \geq 0\}} \left\{ \kappa_{z,t} - \tau \frac{\partial \log Z(\boldsymbol{\mu}_t, \boldsymbol{\lambda}_t, \boldsymbol{\kappa}_t)}{\partial \kappa_z} \right\} \\ &\quad z \in \{-1, +1\},\end{aligned}$$

where  $\text{proj}_{\{x: 0 \leq x \leq C\}}\{w\} \equiv \min(\max(x, 0), C)$  defines the projection of  $x$  on the feasible set  $\{z : 0 \leq z \leq C\}$  via clipping and  $\psi, \varphi, \tau > 0$  define the learning rate.

5: **end for**

**Output:** Assign label for test sample  $\mathbf{x}_m \in \mathcal{D}_s$  as

$$y^* = \text{sign} \left\{ \sum_{n \in T} \hat{\eta}_n \lambda_n^* y_n K(\mathbf{x}_m, \mathbf{x}_n) \right\}, \quad \mathbf{x}_m \in \mathcal{D}_s$$

where  $\hat{\eta}_n = \mathbb{E}[\eta_n | f]$  at the final iteration of step 4.

---

To implement Gibbs sampler under fixed dual parameter  $(\boldsymbol{\lambda}, \boldsymbol{\mu}, \boldsymbol{\kappa})$ , the following procedure is applied iteratively

- Assume the initial value  $\boldsymbol{\eta}_0 = [1, \dots, 1]^T$ .
- For each  $t = 1, 2, \dots, T_G$  or until convergence
  - 1) Given  $\boldsymbol{\eta}_{t-1}$ , generate (random) classification decision value  $f_t(\mathbf{x}_n), n = 1, \dots, N$  according to the Gaussian process (20).
  - 2) Given  $f$ , generate latent variables  $\eta_{n,t}$  according to the formula (19) for each  $n$  independently. Let  $\boldsymbol{\eta}_t \equiv [\eta_{n,t}, n \in T]^T$ .
- Accumulate the expectation value in (21), (22), (23) for the generated pair  $(\boldsymbol{\eta}_t, \mathbf{d}_t)_{t=1, \dots, T_G}$ .

Finally, a complete description of algorithm is presented in **Algorithm 1** based on the framework of projected stochastic gradient descent [26]. In specific, the gradient of dual variables can be approximated via Gibbs sampling as discussed above. As for the constraints on the dual variable  $\lambda_n \in [0, C_1]$ , a *clipping* procedure  $\text{proj}_{\{w: 0 \leq w \leq C\}}\{w\} \equiv \min(\max(w, 0), C)$  should be applied on each move, which is similar to the SVM algorithm [27]. This procedure defines the projection of  $w$  onto the feasible set  $\{w : 0 \leq w \leq C\}$ . Note that in order to maintain the gradient information at each step, the learning rate  $(\psi, \varphi, \tau)$  should be small.

### Remark

- 1) It is seen from (19) and (20) that the role of the dual variables  $(\eta_n, \mu_c)$  is to balance the classification margin  $y f(\cdot)$  and local entropy  $h$  in determining the anomalies.

It reflects an observation that a given sample is more likely to be anomalous, when the margin at a given sample is large and it resides in a low-entropy region simultaneously.

- 2) Given the latent weight  $\boldsymbol{\eta}$ ,  $\hat{f} = \sum_{n \in T} \lambda_n \eta_n y_n K(\cdot, \mathbf{x}_n)$  can be computed using many off-shelf SVM algorithms (e.g. LibSVM [27]).

### B. Prediction and detection on test samples

Similar to (4) for MED, the prediction of GEM-MED is given by

$$\begin{aligned}y^* &= \text{argmax}_y \left\{ \int y f(\mathbf{x}_m) q(f | \hat{\boldsymbol{\eta}}, \mathcal{D}_t) df \right\}, \\ &= \text{sign} \left\{ \sum_{n \in T} \hat{\eta}_n \lambda_n^* y_n K(\mathbf{x}_m, \mathbf{x}_n) \right\} \quad \mathbf{x}_m \in \mathcal{D}_s.\end{aligned}\quad (24)$$

where  $\hat{\boldsymbol{\eta}} \equiv \mathbb{E}[\boldsymbol{\eta} | \mathcal{D}] = [\hat{\eta}_1, \dots, \hat{\eta}_N]^T$  is the conditional estimator of  $\boldsymbol{\eta}$  given by the final loop of Gibbs sampler.

To find the anomalies given  $\hat{\boldsymbol{\eta}}$ , first we could identify the rejection region  $\mathcal{D}_t^{nom}(\hat{\boldsymbol{\eta}}) \equiv \{\mathbf{x}_n : \hat{\eta}_n > 0\} = \mathcal{D}_t \cap \Omega_{1-\beta}$ . Then using this data to form a nominal set and for each test sample, we simply compute the sum of all k-nearest neighbor distances  $R_k(\mathbf{x}_m)$  relative to  $\mathcal{D}_t^{nom}(\hat{\boldsymbol{\eta}})$ . A ME test is simply to claim  $\mathbf{x}_m$  is anomalous if  $R_k(\mathbf{x}_m) > \vartheta$ ; to claim it is nominal if  $R_k(\mathbf{x}_m) \leq \vartheta$ . Here  $\vartheta$  is given by  $\sup_{n \in \mathcal{D}_t^{nom}(\hat{\boldsymbol{\eta}})} R_k(\mathbf{x}_n)$ .

## V. EXPERIMENTS

We illustrate the performance of GEM-MED algorithm on simulated data set as well as on a real data set consisting of acoustic signals. For all data sets, we perform binary classification and anomaly detection simultaneously and the results of SVM method (implemented by LibSVM library [27]), the Robust-Outlier-Detection (i.e. ROD, proposed by et al. [7]) and the GEM-MED algorithm are compared.

### A. Simulated data

To obtain a simulated data set, for each class  $c \in \{ \pm \}$  we generate samples from the bivariate Gaussian distribution  $\mathcal{N}(\mathbf{m}_{+1}, \Sigma)$  and  $\mathcal{N}(\mathbf{m}_{-1}, \Sigma)$ , with mean  $\mathbf{m}_{-1}$   $(3, 3)$  and  $\mathbf{m}_{+1} = -\mathbf{m}_{-1}$  and common covariance  $\Sigma = \begin{bmatrix} 20 & 16 \\ 16 & 20 \end{bmatrix}$ . In these experiments, the linear discriminant function  $\mathcal{L}_C(\mathbf{x}; \Theta) = \mathbf{w}^T \mathbf{x} + b$  is applied, where  $\Theta = (\mathbf{w}, b)$ . Assume the prior  $p_0(\Theta) = \mathcal{N}(\mathbf{w}; \mathbf{0}, \sigma_w^2 \mathbf{I}) \mathcal{N}(b; 0, \sigma_b^2)$ . For each sample  $n$ , the prior on  $\eta_n$  is set to be equally likely  $p_0(\eta_n) = 1/2$ .

The anomalies in the training set are drawn uniformly from a ring with an inner radius of  $R$  and outer radius  $R + \epsilon$  where  $R$  was assigned as one of the values [15, 35, 55, 70] and served as the indication of the noise level in the corrupt training set [7]. The samples then were labeled with event probability. The size of the training set is 100 for each class with ratio of anomaly samples denoted as  $r_a$ . The test set contains 2000 nominal samples from each class. See Fig. (a) for an illustration of the data set.

We first compare the classification accuracy of SVI-Robust-Outlier-Detection (ROD) with outlier parameter  $\rho \in [0.01, 1]$  and GEM-MED, under noise level  $R \in [15, 35, 55, 75]$  and corruption rate  $r_a = [0.2, 0.3, 0.4, 0.5]$ . In implementation of the GEM-MED method, we apply the bipartite kNNG to approximate the local entropy, where the parameter  $k = 5$ , intrinsic dimension  $d = 2$ . To update the dual variables  $(\lambda, \mu, \kappa)$ , the learning rate  $\psi \in [1, 5] \times 10^{-3}$ ,  $\varphi \in [1, 5] \times 10^{-2}$ ,  $\tau \in [1, 5] \times 10^{-2}$ . For ROD, we choose the outlier parameter  $\rho \in \{0.02, 0.2, 0.6\}$  for comparison, while  $\rho = 0.02$  is the best for  $\forall \rho \in [0.01, 1]$ . All the parameters are tuned via a 5-fold-cross-validation procedure.

The experiments are run for 50 times to compute the mean and standard deviation of the test errors for these models. Fig. 5(a) shows the test error (%) versus various noise level  $R$  (with  $r_a = 0.2$ ), and Fig. 5(b) shows the test errors under different corruption rate settings (with  $R = 55$ ). In both experiments, GEM-MED outperforms ROD and SVM in terms of classification accuracy. Note that when the noise level or the corruption rate increases, the training data become less representative of the test data and the difference between their distributions increases. This causes a significant performance deterioration for MED/SVM method, which is demonstrated in Fig. 5(a) and Fig. 5(b). Fig. 4 (b) also shows the bias of SVM

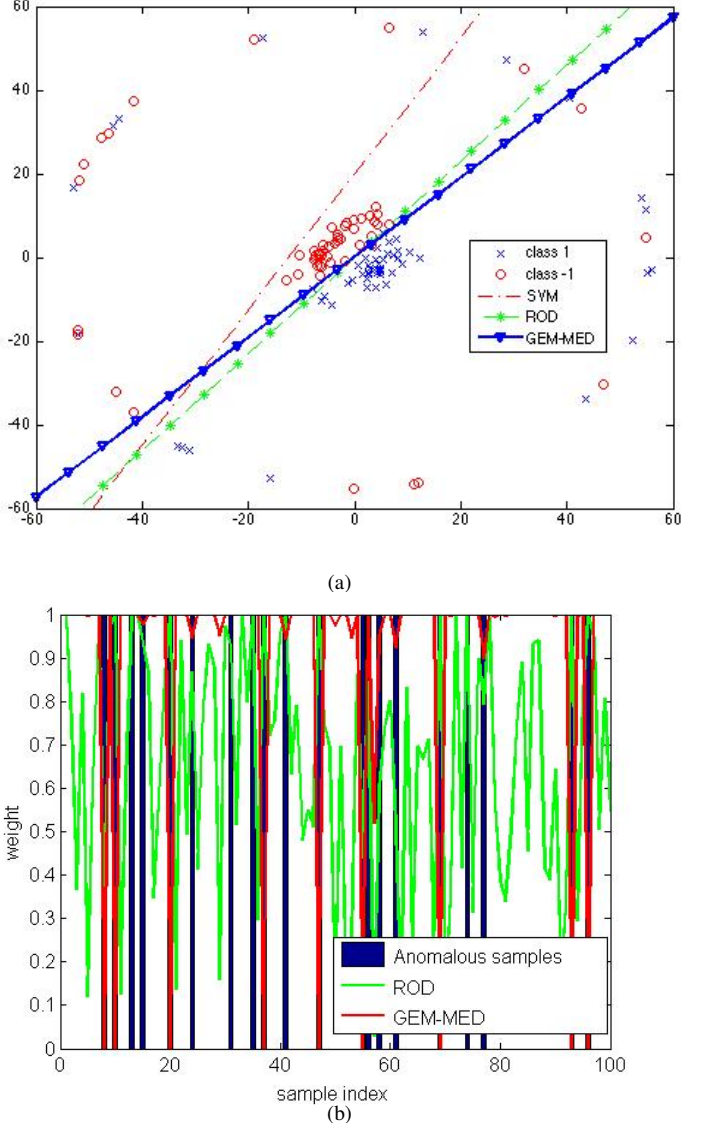


Fig. 4. (a) The classification decision boundary for SVM, ROD and GEM-MED on the simulated data set with two bivariate Gaussian distribution  $\mathcal{N}(\mathbf{m}_{+1}, \Sigma)$ ,  $\mathcal{N}(\mathbf{m}_{-1}, \Sigma)$  in the center and a set of anomalous samples for both classes distributed in a ring. Note that SVM is biased toward the anomalies and ROD and GEM-MED are insensitive to the anomalies. (b) The Illustration of anomaly score  $\hat{\eta}_n$  for GEM-MED and ROD. The GEM-MED is more accurate than ROD in term of anomaly detection.

classifier towards the anomalies in the outer ring. Comparing GEM-MED and ROD with SVM using Fig 5(a) and Fig. 5(b), because both ROD and GEM-MED limit the maximal loss values during training, these two methods avoid over-fitting to anomalies. Moreover, since the GEM-MED model takes into account for the local distribution for each training sample, it is more adaptive to anomalies in the training set, as opposed to ROD, which does not apply any prior knowledge about the nominal distribution but only relies on the predefined outlier parameter  $\rho$  to limit the training loss.

Since both ROD and GEM-MED method can detect the anomalies in the training set, we examine their efficiency, under the fixed corruption rate 0.2. In ROD, the weight  $\eta_n \in [0, 1]$  for each sample can be used to infer the likelihood

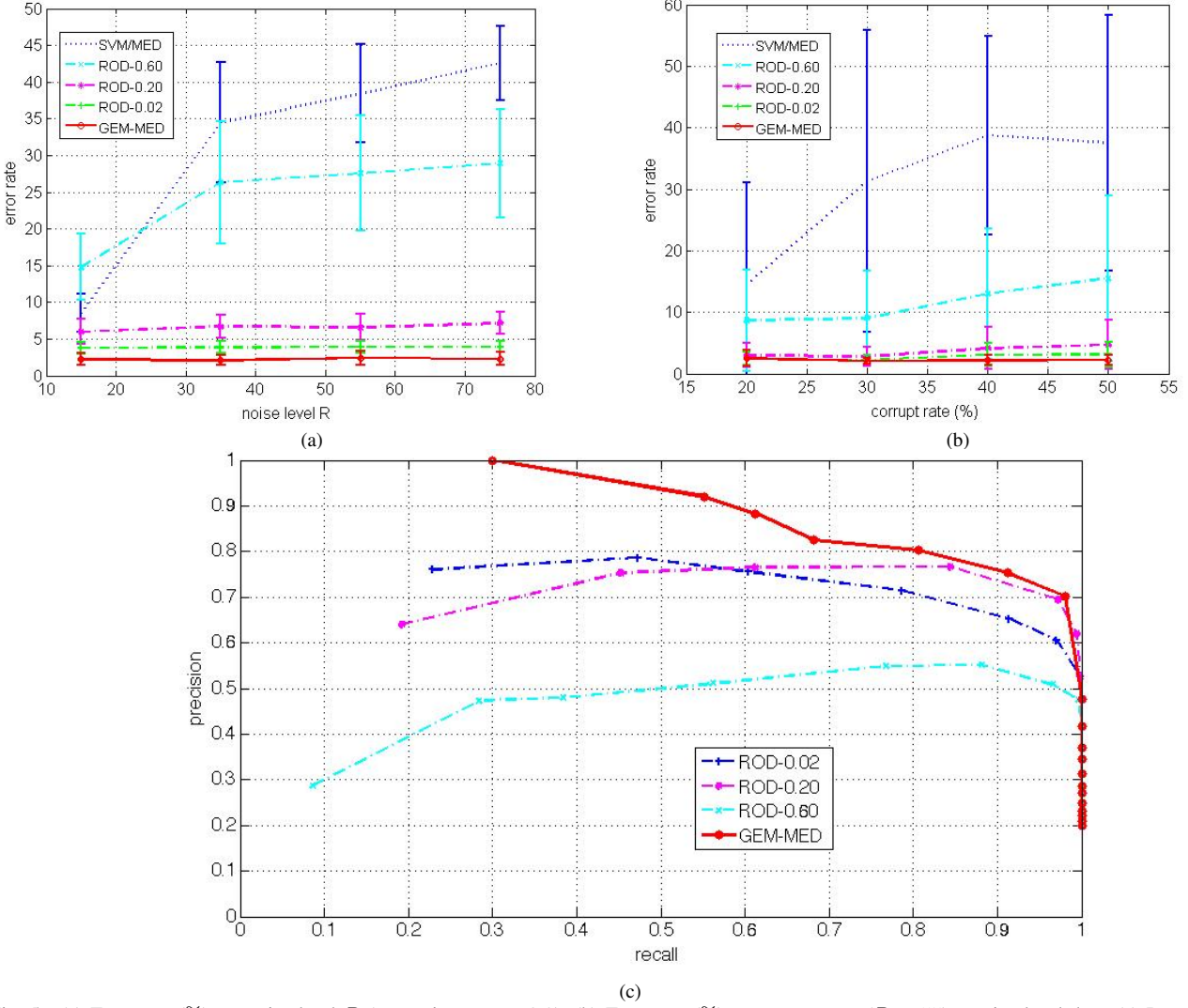


Fig. 5. (a) Test error (%) vs. noise level  $R$  (corruption rate = 0.2). (b) Test error (%) vs. corrupt rate ( $R = 55$ ) on simulated data. (c) Recall-precision curve for GEM-MED and RODs on simulated data (corruption rate = 0.2). From (a) and (b), GEM-MED slightly outperforms both MED/SVM and ROD for various  $\rho$  in classification accuracy, when either noise level or corrupt rate increases. From (c), we see that under the same corruption rate, GEM-MED surpleses ROD due to the superiority of GEM constraints in anomaly detection.

of anomalies, while in GEM-MED, the conditional estimate  $\hat{\eta}_n = \mathbb{E}[\eta_n | \mathbf{w}, \mathcal{D}]$  is obtained at the final iteration of the Gibbs sampling. Following the procedure in [7], these anomaly scores are placed in ascending order. We compute the precision and recall using this ordering and take average of 50 runs. The precision and recall measure are defined as

$$\begin{aligned} \text{precision} &= \frac{|\{n : \eta_n \leq \rho_c\} \cap \{n : (\mathbf{x}_n, y_n) \text{ are anomalous}\}|}{|\{n : \eta_n \leq \rho_c\}|} \\ \text{recall} &= \frac{|\{n : \eta_n \leq \rho_c\} \cap \{n : (\mathbf{x}_n, y_n) \text{ are anomalous}\}|}{|\{n : (\mathbf{x}_n, y_n) \text{ are anomalous}\}|}, \end{aligned}$$

where the threshold  $\rho_c$  is the cut-off rank that varies at each run. Both precision and recall are measures of relevancy in anomaly detection. Fig.5(c) plots the precision versus recall curve for various RODs and GEM-MED, with a snapshot of a typical result illustrated in Fig.4(c). As seen in both figures,

as more true anomalous samples are retrieved (, which means that the recall increases), the GEM-MED method enjoys higher percentage of true anomalies in all detected samples (, i.e. higher precision), compared to that given by ROD method with the optimal outlier parameter (i.e.  $\rho = 0.20$  in plot). In other word, the detector embedded in GEM-MED model is more efficient than that of ROD. This is because the anomalies distributed in the outer ring resides in the high entropy region, as assumed in GEM principle. The GEM-MED, thus, has better performance in terms of the efficiency and accuracy of anomaly detection than does ROD.

#### B. Footstep classification data set

We perform experiments on a real data set collected by the U.S. Army Research Lab [23], [24], [28]. This data set contains footstep signals recorded by a multisensor system, which includes four acoustic sensors and three seismic sensors.

All the sensors are well-synchronized and operates in a natural environment, where the environmental noise and multiple sensor failures corrupted the acoustic signal recordings. The task is to discriminate between human footsteps and human-leading animal footsteps. We use the signals collected via four acoustic sensors (labeled as Sensor 1,2,3,4) to perform the classification, since it is easy to virtually identify sensor failures as anomalies based on the acoustic waveform. See Fig. 6 for a snapshot of human footsteps recorded by four acoustic sensors. It is noticed that the fourth acoustic suffered from sensor failure and the magnitude of the waveform is very small. The data set involves 84 human subjects and 66 human-animal subjects. We randomly selected 25 subjects from each class as the training set, with the rest designated as the test set.

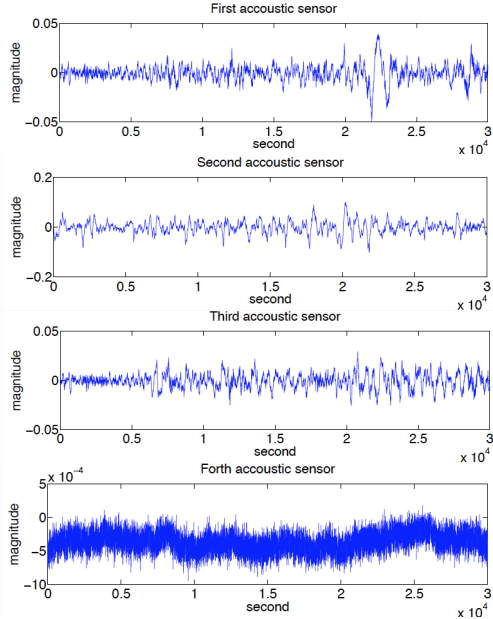


Fig. 6. A snapshot of human footprint collected by four well-synchronized acoustic sensors.

In the preprocessing step, the location with strongest signal response are identified and signals within a fixed size of window (i.e. 23 sec.) are extracted from the background noises. Each individual footprint signal is then separated into ten 75% overlapping segments to capture local signal information. Each segment has 15,000 samples corresponding to 1.5 seconds of the signal and each record generates 20 segments. Fig. 7 shows the power spectrogram (dB) as a function of time (sec.) and frequency (Hz.) for human footsteps and human-leading animal footsteps. The majority of energy for both footsteps are concentrated in low frequency band and one may observe the difference of period of successive steps between these two classes of signals. To summarize the characteristic of the power spectrogram, we extract a mel-frequency cepstral coefficients (MFCCs, [29]) vector with 50 msec. windows at a 10 msec. rate for each segment. The first 13 coefficients were retained for each frame and concatenated along the whole segment, which results in a 200 dimensional feature vector. We then apply PCA to reduce the dimensionality from 200 to 50, while preserving 85% of the total energy, as in [24], [28].

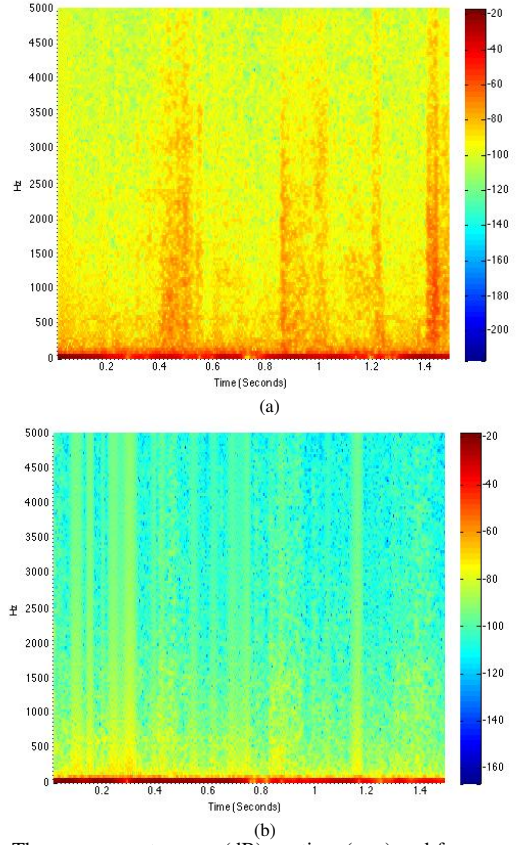


Fig. 7. The power spectrogram (dB) vs. time (sec.) and frequency (Hz.) for human footprint (a) and human-leading animal footprint (b). Observed that the period of successive steps is one feature to separate these two signals.

In these experiments, we compare performance of kernel SVM, kernel MED, ROD for outlier parameter  $\rho \in [0.01, 1]$  and GEM-MED using four individual sensors as well as the combination of four sensors together, where an augmented feature of dimension  $50D$  is constructed via feature concatenation. For all of the above methods, the Gaussian kernel  $K(\mathbf{x}_i, \mathbf{x}_j) = \exp(-\gamma \|\mathbf{x}_i - \mathbf{x}_j\|_2^2)$  is applied and the kernel parameter  $\gamma > 0$  is tuned via 5-fold-cross-validation. A Gaussian Process  $\mathcal{N}(\mathbf{w}; \mathbf{0}, \mathbf{I})$  is used as prior on  $\mathbf{w}$  for kernel MED and GEM-MED method. For each sample  $n$ , the prior on  $\eta_n$  is set to  $p_0(\eta_n) = 1/2$ . Also, BP-kNNG is applied to estimate the local entropy on the transformed feature space with  $k = 10$  and intrinsic dimension  $d$  estimated from the sample distribution.

Table II shows the classification accuracy of above methods for four individual sensors and the combination of all four sensors. For ROD only  $\rho = 0.02$  and  $\rho = 0.20$  are shown, while  $\rho = 0.20$  is the best for  $\forall \rho \in [0.01, 1]$ . It is seen that the GEM-MED method outperforms all of the ROD- $\rho$  algorithms and also outperforms kernel MED in classification accuracy for sensor 1,2,4. Notice that neither kernel MED nor kernel SVM is resistant to the sensor failures in the data set, which explains their poor accuracy in sensor 3 and sensor 4. These two methods are comparable, since the kernel MED classifier can be seen as an average of multiple kernel SVM classifiers, which reduce the standard deviation of the classifier. Moreover, as noted in Table II, we also compare GEM-MED with a two-

TABLE II  
CLASSIFICATION ACCURACY WITH DIFFERENT SENSORS, WITH THE BEST PERFORMANCE SHOWN IN **BOLD**.

Classification Accuracy (%) mean $\pm$ standard error						
sensor no.	kernel SVM	kernel MED	ROD-0.02	ROD-0.2	GEM + SVM	GEM-MED
1	$71.2 \pm 8.2$	$71.1 \pm 5.3$	$73.7 \pm 3.7$	$76.0 \pm 2.5$	$72.5 \pm 4.2$	<b><math>78.4 \pm 3.3</math></b>
2	$60.8 \pm 12.5$	$62.3 \pm 10.2$	$71.5 \pm 7.3$	$76.5 \pm 5.3$	$70.3 \pm 2.5$	<b><math>82.1 \pm 3.1</math></b>
3	$60.5 \pm 14.2$	$60.0 \pm 13.1$	$63.2 \pm 5.4$	<b><math>67.6 \pm 4.2</math></b>	$56.5 \pm 3.5$	$66.8 \pm 4.5$
4	$59.6 \pm 10.1$	$58.4 \pm 8.2$	$71.8 \pm 7.2$	$73.2 \pm 4.2$	$76.5 \pm 2.7$	<b><math>80.1 \pm 3.1</math></b>
1,2,3,4	$75.9 \pm 7.5$	$78.6 \pm 5.1$	$79.2 \pm 3.7$	$79.8 \pm 2.5$	$75.2 \pm 3.3$	<b><math>84.0 \pm 2.3</math></b>

stage procedure that concatenates the GEM anomaly detector with the SVM classifier. At the first stage, the GEM anomaly detector approximates the minimal-entropy-set of false alarm level  $\beta$  using corrupted samples and then at the second stage, the SVM classifier is learned based on the filtered data set. To be fair in comparison, we reweighted each error by the ratio  $N_f/N$ , where  $N_f$  is the size of filtered data set. In Table II, the two stage learning approach is not preferred in highly corrupted sensor 3 and sensor 4. A reasonable explanation is that when the GEM detector is learned without inferring the classification margin, it cannot effectively limit the negative influence of those corrupted samples that are close to the class boundary. As a consequence, the classifier is still vulnerable to these anomalies. This indicates the superiority of joint classification and detection as compared with a typical two-stage approach in practice.

Table III shows the anomaly detection accuracies for ROD and GEM-MED. It demonstrates a significant improvement in detection for sensor 1,3,4 for GEM-MED. Note that ROD-0.2 has higher detection accuracy than GEM-MED in sensor 2, since many anomalous samples in this sensor reside in the high density region of the data set, which violates the sparse anomaly assumption underlying GEM. In the case of the concatenated features from all four sensors, as most of the anomalies based on the joint feature representation reside in the high entropy region of the data set, GEM-MED is able to successfully detect most of the anomalous samples.

## VI. CONCLUSION AND FUTURE WORK

In this paper we propose the GEM-MED algorithm that provides a unified optimization framework for classification and anomaly detection. We demonstrate its performance advantages in terms of both classification accuracy and detection rate on a simulated data set and a real footstep data set, as compared to the anomaly-blind Ramp-Loss-based classification method. The work presented in this paper is also related to a well-investigated area called *domain adaptation*, where the training and test distribution, by assumption, are different. Compared to the classical work in domain adaptation, such

TABLE III  
ANOMALY DETECTION ACCURACY WITH DIFFERENT SENSORS, WITH THE BEST PERFORMANCE SHOWN IN **BOLD**.

Anomalous Detection Accuracy (%) mean $\pm$ standard error			
sensor no.	ROD-0.02	ROD-0.2	GEM-MED
1	$30.2 \pm 1.3$	$59.0 \pm 3.5$	<b><math>70.5 \pm 1.3</math></b>
2	$23.5 \pm 2.6$	<b><math>63.5 \pm 2.8</math></b>	$63.4 \pm 2.5$
3	$5.3 \pm 1.4$	$48.1 \pm 3.3$	<b><math>72.8 \pm 1.5</math></b>
4	$22.8 \pm 3.2$	$65.2 \pm 4.2$	<b><math>88.1 \pm 2.1</math></b>
1,2,3,4	$38.5 \pm 6.3$	$63.3 \pm 5.5$	<b><math>88.5 \pm 4.1</math></b>

as *covariate shift* [30]–[33] or *sample selection bias* [34], our method also applies the instance reweighting technique. However, in our setting, the weight is closely related but is not equal to the ratio of test distribution versus training distribution, since it also utilize the classification margin in inferring the weights. Moreover, it can be shown that the support vector machine does not satisfy the basic assumption in covariate shift, i.e. the conditional distribution  $p(y|x)$  will change when the marginal distribution  $p(x)$  make changes. It is interesting to investigate the relationship between our method and the covariate shift methods and it could be our future work.

## VII. ACKNOWLEDGE

Tianpei Xie is partially supported by ARO grant WA11NF-11-1-103A1. Thanks to the U.S. Army Research Lab. for providing the multi-sensor data set. Also Tianpei Xie thanks the support of Xu LinLi for providing the code for Robust-Outlier-Detection algorithm and Kumar Sricharan for providing code to implement the Geometric Entropy Minimization algorithm based on BP-kNNG.

## APPENDIX

## A. Proof of proposition 4.1

**Proof:** The Lagrangian functional is given as

$$\begin{aligned} \mathcal{L}(q, \boldsymbol{\lambda}, \boldsymbol{\mu}, \boldsymbol{\nu}) &= \mathbb{E}_q [\log q - \log p_0] + \sum_{n \in T} \lambda_n \mathbb{E}_q [\eta_n \mathcal{L}_C] - \sum_{z \in \{\pm 1\}} \mu_z \mathbb{E}_q [\tilde{\mathcal{L}}_{D,z}] \\ &\quad - \sum_{z \in \{\pm 1\}} \kappa_z \mathbb{E}_q \left[ \sum_{n: y_n = z} \eta_n / |T| - \beta \right] \end{aligned}$$

with dual variables  $\boldsymbol{\lambda} = \{\lambda_n, n \in T\} \succeq \mathbf{0}$ ,  $\boldsymbol{\mu} = (\mu_z, z \in \{\pm 1\}) \succeq \mathbf{0}$  and  $\boldsymbol{\nu} \geq \mathbf{0}$ .

Then the result follows directly from solving a system of equations according to the KKT condition.  $\blacksquare$

## B. Proof of proposition 4.2

**Proof:** According to [2], the dual optimization is given as

$$\begin{aligned} \max_{\boldsymbol{\lambda}, \boldsymbol{\mu}, \boldsymbol{\kappa} \geq 0} & -\log Z(\boldsymbol{\lambda}, \boldsymbol{\mu}, \boldsymbol{\kappa}) \\ &= -\log \prod_{n \in T} \int \exp(-c(1 - \xi_n) - \lambda_n \xi_n) d\xi_n \\ &\quad \times \int \int \exp \left( -\frac{1}{2} \mathbf{f}^T \mathbf{K}^{-1} \mathbf{f} + \sum_n \lambda_n \eta_n y_n f_n \right) d\mathbf{f} \\ &\quad \times p_0(\boldsymbol{\eta}) \exp \left( -\sum_{z \in \{\pm 1\}} \mu_z \sum_{n: z} \eta_n \hat{h}_{n,T} + \sum_{z \in \{\pm 1\}} \mu_z \hat{\gamma}_z \right. \\ &\quad \quad \left. + \sum_{z \in \{\pm 1\}} \kappa_z \sum_{n: z} \eta_n + \sum_{z \in \{\pm 1\}} \kappa_z \beta \right) d\boldsymbol{\eta} \\ &= \sum_{n \in T} (\lambda_n + \log(1 - \lambda_n/c)) - \sum_{z \in \{\pm 1\}} \mu_z \hat{\gamma}_z - (\sum \kappa_z) \beta \\ &\quad - \log \int \exp \left( \frac{1}{2} Q(\mathbf{K}, (\boldsymbol{\lambda} \odot \boldsymbol{\eta} \odot \mathbf{y})) + \boldsymbol{\eta}^T (-\boldsymbol{\mu} \otimes \hat{\mathbf{h}} + \boldsymbol{\kappa} \otimes \mathbf{e}) \right) \\ &\quad \quad \times p_0(\boldsymbol{\eta}) d\boldsymbol{\eta} \end{aligned}$$

where

$$\begin{aligned} Q(\mathbf{K}, \mathbf{x}) &= \mathbf{x}^T \mathbf{K} \mathbf{x} \\ Q(\mathbf{K}, (\boldsymbol{\lambda} \odot \boldsymbol{\eta})) &\equiv (\boldsymbol{\lambda} \odot \boldsymbol{\eta})^T \mathbf{K} (\boldsymbol{\lambda} \odot \boldsymbol{\eta}) \\ &= \boldsymbol{\lambda}^T (\mathbf{K} \odot (\boldsymbol{\eta} \boldsymbol{\eta}^T)) \boldsymbol{\lambda} \\ &= Q(\mathbf{K}(\boldsymbol{\eta}), \boldsymbol{\lambda}). \end{aligned}$$

$\blacksquare$

## C. Proof of proposition 4.3

**Proof:** The expression for  $q(\tilde{\Theta})$  is given as

$$\begin{aligned} q(\tilde{\Theta}) &\propto \exp \left( -\frac{1}{2} \mathbf{f}^T \mathbf{K}^{-1} \mathbf{f} + \sum_n \lambda_n \eta_n y_n f_n \right) \\ &\quad \times p_0(\boldsymbol{\eta}) \exp \left( -\sum_{z \in \{\pm 1\}} \mu_z \sum_{n: z} \eta_n \hat{h}_{n,T} + \sum_{z \in \{\pm 1\}} \kappa_z \sum_{n: z} \eta_n \right) \end{aligned}$$

$$\begin{aligned} &\times \prod_{n \in T} \exp(-c + (c - \lambda_n) \xi_n) \\ &= q(f, \boldsymbol{\eta}) \prod_n q(\xi_n) \end{aligned}$$

Given all  $\eta_n, n \in T$ ,

$$\begin{aligned} q(f|\boldsymbol{\eta}) &\propto \exp \left( -\frac{1}{2} \mathbf{f}^T \mathbf{K}^{-1} \mathbf{f} + \sum_n (\lambda_n \eta_n) f_n \right) \\ &= \exp \left( -\frac{1}{2} (\mathbf{f} - \mathbf{K}(\boldsymbol{\lambda} \odot \boldsymbol{\eta} \odot \mathbf{y}))^T \mathbf{K}^{-1} (\mathbf{f} - \mathbf{K}(\boldsymbol{\lambda} \odot \boldsymbol{\eta} \odot \mathbf{y})) \right) \\ &= \mathcal{N}(\mathbf{K}(\boldsymbol{\lambda} \odot \boldsymbol{\eta} \odot \mathbf{y}), \mathbf{K}). \end{aligned}$$

On the other hand, given  $f, \boldsymbol{\eta} = (\eta_n, n \in T)$  are fully separated in above formula, therefore  $q(\boldsymbol{\eta}|f) = \prod_n q(\eta_n|f)$ .  $\blacksquare$

## REFERENCES

- [1] B. Schölkopf and A. J. Smola, *Learning with kernels*. The MIT Press, 2002.
- [2] T. Jaakkola, M. Meila, and T. Jebara, “Maximum entropy discrimination,” *Advances in Neural Information Processing Systems*, 1999.
- [3] P. L. Bartlett and S. Mendelson, “Rademacher and Gaussian complexities: Risk bounds and structural results,” *The Journal of Machine Learning Research*, vol. 3, pp. 463–482, 2003.
- [4] O. Bousquet and A. Elisseeff, “Stability and generalization,” *The Journal of Machine Learning Research*, vol. 2, pp. 499–526, 2002.
- [5] M. Yang, L. Xu, M. White, D. Schuurmans, and Y.-l. Yu, “Relaxed clipping: A global training method for robust regression and classification,” in *Advances in neural information processing systems*, 2010, pp. 2532–2540.
- [6] B. Schölkopf, R. C. Williamson, A. J. Smola, J. Shawe-Taylor, and J. C. Platt, “Support vector method for novelty detection,” *Advances In Neural Information Processing Systems*, vol. 12, pp. 582–588, 1999.
- [7] L. Xu, K. Crammer, and D. Schuurmans, “Robust support vector machine training via convex outlier ablation,” *AAAI*, vol. 6, pp. 536–542, 2006.
- [8] C. D. Scott and R. D. Nowak, “Learning minimum volume sets,” *The Journal of Machine Learning Research*, vol. 7, pp. 665–704, 2006.
- [9] A. O. Hero, “Geometric entropy minimization (GEM) for anomaly detection and localization,” *Advances in Neural Information Processing Systems*, pp. 585–592, 2006.
- [10] K. Sricharan and A. Hero, “Efficient anomaly detection using bipartite k-NN graphs,” *Advances in Neural Information Processing Systems*, pp. 478–486, 2011.
- [11] J. Blitzer, R. McDonald, and F. Pereira, “Domain adaptation with structural correspondence learning,” in *Proceedings of the 2006 conference on empirical methods in natural language processing*. Association for Computational Linguistics, 2006, pp. 120–128.
- [12] V. Chandola, A. Banerjee, and V. Kumar, “Anomaly detection: A survey,” *ACM Computing Surveys (CSUR)*, vol. 41, no. 3, p. 15, 2009.
- [13] H. Daume III and D. Marcu, “Domain adaptation for statistical classifiers,” *Journal of Artificial Intelligence Research*, pp. 101–126, 2006.
- [14] D. E. Tyler, “Robust statistics: Theory and methods,” *Journal of the American Statistical Association*, vol. 103, no. 482, pp. 888–889, 2008.
- [15] N. Krause and Y. Singer, “Leveraging the margin more carefully,” *Proceedings of the twenty-first international conference on Machine learning*, p. 63, 2004.
- [16] H. Masnadi-Shirazi and N. Vasconcelos, “On the design of loss functions for classification: theory, robustness to outliers, and savageboost,” in *Advances in neural information processing systems*, 2009, pp. 1049–1056.
- [17] Y. Wu and Y. Liu, “Robust truncated hinge loss support vector machines,” *Journal of the American Statistical Association*, vol. 102, no. 479, 2007.
- [18] P. M. Long and R. A. Servedio, “Random classification noise defeats all convex potential boosters,” *Machine Learning*, vol. 78, no. 3, pp. 287–304, 2010.

- [19] Q. Song, W. Hu, and W. Xie, "Robust support vector machine with bullet hole image classification," *Systems, Man, and Cybernetics, Part C: Applications and Reviews, IEEE Transactions on*, vol. 32, no. 4, pp. 440–448, 2002.
- [20] L. Wang, H. Jia, and J. Li, "Training robust support vector machine with smooth ramp loss in the primal space," *Neurocomputing*, vol. 71, no. 13, pp. 3020–3025, 2008.
- [21] T. Jebara, "Multitask sparsity via maximum entropy discrimination," *The Journal of Machine Learning Research*, vol. 12, pp. 75–110, 2011.
- [22] T. Damarla, A. Mehmood, and J. Sabatier, "Detection of people and animals using non-imaging sensors," *Information Fusion (FUSION), 2011 Proceedings of the 14th International Conference on*, pp. 1–8, 2011.
- [23] T. Damarla, "Seismic and ultrasonic data analysis for characterizing people and animals," *SPIE Defense, Security, and Sensing*, 2012.
- [24] P.-S. Huang, T. Damarla, and M. Hasegawa-Johnson, "Multi-sensory features for personnel detection at border crossings," *Information Fusion (FUSION), 2011 Proceedings of the 14th International Conference on*, pp. 1–8, 2011.
- [25] J. Zhu, N. Chen, and E. P. Xing, "Infinite latent SVM for classification and multi-task learning," *Advances in Neural Information Processing Systems*, pp. 1620–1628, 2011.
- [26] D. P. Bertsekas, *Nonlinear programming*. Athena Scientific, 1999.
- [27] C.-C. Chang and C.-J. Lin, "LIBSVM: a library for support vector machines," *ACM Transactions on Intelligent Systems and Technology (TIST)*, vol. 2, no. 3, p. 27, 2011.
- [28] N. H. Nguyen, N. M. Nasrabadi, and T. D. Tran, "Robust multi-sensor classification via joint sparse representation," *Information Fusion (FUSION), 2011 Proceedings of the 14th International Conference on*, pp. 1–8, 2011.
- [29] P. Mermelstein, "Distance measures for speech recognition, psychological and instrumental," *Pattern recognition and artificial intelligence*, vol. 116, pp. 374–388, 1976.
- [30] J. Quiñonero-Candela, M. Sugiyama, A. Schwaighofer, and N. D. Lawrence, *Dataset shift in machine learning*. The MIT Press, 2009.
- [31] H. Daumé III, "Frustratingly easy domain adaptation," *arXiv preprint arXiv:0907.1815*, 2009.
- [32] J. Huang, A. Gretton, K. M. Borgwardt, B. Schölkopf, and A. J. Smola, "Correcting sample selection bias by unlabeled data," in *Advances in neural information processing systems*, 2006, pp. 601–608.
- [33] S. Bickel, M. Brückner, and T. Scheffer, "Discriminative learning for differing training and test distributions," in *Proceedings of the 24th international conference on Machine learning*. ACM, 2007, pp. 81–88.
- [34] C. Cortes, M. Mohri, M. Riley, and A. Rostamizadeh, "Sample selection bias correction theory," in *Algorithmic Learning Theory*. Springer, 2008, pp. 38–53.